The Effect of *In situ* Magnetic Field on Magnetic Properties and Residual Stress of Fe-Based Amorphous Film

Sibo Wang[1,2], Hoe Joon Kim[3], Jun Chen[1], David E. Laughlin[2,4], Gianluca Piazza[2], and Jingxi Zhu[1]

[1]School of Electronic and Information Technology, Sun Yat-sen University, Guangzhou 510006, China
[2]Department of Electrical and Computer Engineering, Carnegie Mellon University, Pittsburgh, PA 15213 USA
[3]Department of Robotics Engineering, Daegu Gyeongbuk Institute of Science and Technology, Daegu 42988, South Korea
[4]Department of Materials Science and Engineering, Carnegie Mellon University, Pittsburgh, PA 15213, USA

Fe-based amorphous thin films of two compositions ($Fe_{80}B_{20}$ and $Fe_{65.6}Co_{9.4}B_{25}$) were deposited by RF magnetron sputtering with and without applying an *in situ* magnetic field along the films' in-plane direction. In addition, films with varying thickness were deposited for each composition. Hysteresis loops and residual stress were measured and compared to study the effect of *in situ* fields on the magnetic and magnetostrictive behavior of the films. Results showed that *in situ* magnetic fields can lower the in-plane coercivity for the $Fe_{80}B_{20}$ films. Also, when the residual stress was below a certain level, its distribution in different directions shows a uniaxial feature due to the applied *in situ* field. This uniaxial distribution of stress adds an extra magnetoelastic anisotropy to the films. This paper provides insight for optimizing magnetic thin films' properties for applications where the magnetostriction is relevant, in terms of the *in situ* magnetic field, coercivity, and residual stress.

Index Terms— **Anisotropy, coercivity, *in situ* field, magnetostriction, residual stress.**

I. Introduction

MAGNETOSTRICTIVE materials have been of special interest in magnetic sensor applications [1]–[6]. Fe-based magnetostrictive materials (the most commonly used material for magnetic sensors) are normally processed into thin films during nano/micro fabrication [1], [3]–[7]. While much research on Fe-based magnetostrictive materials has centered on their composition and processing optimization in its bulk state [8]–[11], it is necessary to investigate how the process of fabrication, and its consequences, affect the materials' magnetic and mechanical behavior in the thin-film condition [12]. This is critical to enhance the performance of micro/nano scale devices.

There are two fabrication-related factors that can play roles in determining the thin films' properties. First, residual stress and its resulting magnetoelastic anisotropy are inevitable during the deposition for Fe-based magnetostrictive thin films. This could be important for both device fabrication and the magnetostrictive behavior of films [13], [14]. Second, *in situ* magnetic fields are commonly applied during the deposition of the films' to create magnetic anisotropy [4], [7], [15]. Whereas some basics about magnetic anisotropy created by *in situ* field have been studied [7], [15]–[17], its interaction with mechanical behavior of deposited films, such as residual stress, remains an interesting as well as valuable aspect for materials and device optimization. Therefore, the factors mentioned above need to be more clearly understood for the applications of magnetostrictive thin films in magnetic sensors.

Manuscript received August 4, 2017; revised January 14, 2018; accepted February 5, 2018. Date of publication March 15, 2018; date of current version May 16, 2018. Corresponding author: J. Zhu (e-mail: zhjingxi@mail.sysu.edu.cn).

Color versions of one or more of the figures in this paper are available online at http://ieeexplore.ieee.org.

Digital Object Identifier 10.1109/TMAG.2018.2808355

In the following , we focus on the correlation between the *in situ* magnetic field, coercivity, and residual stress in order to provide some insights on how to optimize the properties of such films. Accordingly, this paper is organized as follows. In Section II, experimental procedures, including equipment, deposition process, materials, and characterization tests, will be provided. Then in Section III, results, such as thin-film coercivity, residual stress, and its distribution, will be presented and an explanation of the results will be presented. Finally, in Section IV, we will discuss correlations between *in situ* fields with magnetic and mechanical behavior for such magnetostrictive films based on the results summarized in Section III. This paper is beneficial for future research on the optimization of magnetostrictive thin films and their applications.

II. Experimental Procedures

The $Fe_{80}B_{20}$ (FeB) and $Fe_{65.6}Co_{9.4}B_{25}$ (FeCoB) amorphous thin films were deposited on 4 in standard Si ⟨100⟩ substrates by RF magnetron sputtering in a home-made five-target sputtering system. The alloy targets had nominal compositions of $Fe_{80}B_{20}$ and $Fe_{65.6}Co_{9.4}B_{25}$ and were custom made by Materion, Ltd. Before each deposition, the base pressure of the deposition chamber was ensured to be below 2×10^{-7} Torr. During the deposition, an *in situ* magnetic field of 20 Oe was applied along an in-plane direction of the films. A 5 nm Ta layer was first deposited as the adhesion layer followed by the magnetic film. In order to avoid substrate heating from the plasma as much as possible and to minimize thermal stress, the deposition process was divided into several subcycles: after every 5 min of deposition, the substrate was moved out of the plasma and allowed to cool for 5 min, in addition to the wafer-cooling from substrate table. The maximum temperature of the film during deposition was verified with Tempil labels to be below 50 °C. Different thicknesses

TABLE I
BRIEF SUMMARY OF DEPOSITION CONDITIONS (POWER, PRESSURE, FLOWRATE RANGE, AND DEPOSITION RATE RANGE) FOR $Fe_{80}B_{20}$ AND $Fe_{65.6}Co_{9.4}B_{25}$

Compositions	RF Power (W)	Pressure (mTorr)	Flow rate Range (sccm)	Deposition Rate Range (nm/min)
$Fe_{80}B_{20}$	80; 100; 120	8; 9; 10; 11	42-69.5	1.37-1.97
$Fe_{65.6}Co_{9.4}B_{25}$	80; 100; 120	8; 9; 10; 11	45.4-75.4	1.38-2.25

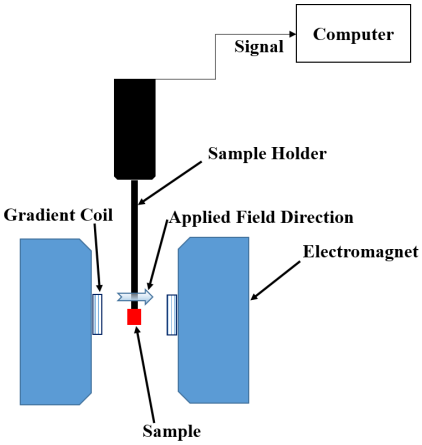

Fig. 1. Schematic of AGFM measurement system.

(150, 250, and 500 nm) were deposited by changing the number of sub-cycles in each deposition. The choice for such a series of thickness is based on previous works related to Fe-based magnetostrictive films [4], [18], [19], as well as limitation of fabrication capability. For each composition, the deposition conditions (power, pressure, deposition rate, and flowrate) are briefly summarized in Table I. For better performance of the magnetic layer in the device, the goal for the film fabrication was to minimize the residual stress while maintaining the amorphous nature of the film and acquiring the necessary magnetic anisotropy.

Theta-2 scans were carried out on the as-deposited films for checking amorphous state by using a Philips X'Pert PRO MRD X-ray diffractometer. The target was Cu and a Ni filter was used during scanning. A 15 mm × 15 mm chip was cut from the center of the Si wafer. In order to capture the potentially low counts from the nano-crystalline phase of low crystallinity, the out-of-plane scan was done at a step size of 0.026° per step, between the range from 10° to 120°. The total scanning time was 4.5 h. During the scanning, two theta angles from 68° to 70° were skipped to prevent the detector from damage due to the intense signal from the primary Si ⟨400⟩ peak.

The hysteresis loops were measured by alternating gradient field magnetometer (AGFM). A schematic of the equipment is shown in Fig. 1. To avoid interference from the circulating ambient air, a plastic cover enclosed the two coils, the sample, its holder, and the head that processed the signal. The sample was usually a 3 mm × 3 mm chip mounted on the sample holder, with films' in-plane direction parallel to the direction of

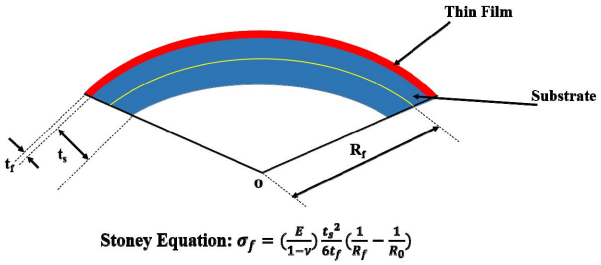

Fig. 2. Schematics of the Stoney method.

the applied field. In measurements, samples were placed with films' *in situ* field direction either parallel or perpendicular to the applied field. The sample was first cleaned and then attached to the sample holder by Vaseline to minimize any potential contamination and noise. The sample holder was placed in the center of the gap between the two gradient coils. After the sample stabilized, the magnetization of the sample was measured with the applied magnetic field changing between ±150 Oe with 1 Oe increment. The signs denoted the change in the applied field direction. Finally, hysteresis loops were plotted with normalized magnetization and from which properties such as coercivity and remnant magnetization can be extracted.

The residual stress of the films and its distribution along different directions across the wafer were measured by a scanning laser film stress measurement system. Since the thickness of the films deposited (500 nm max.) was significantly less than that of the substrate (i.e., 525 μm), the Stoney method [20] was adopted. The residual stress was obtained by using the "Stoney equation" with the measured substrate curvature data, as shown in Fig. 2, where E and ν are Young's modulus and Poison's ratio of the substrate, respectively, R_f and R_0 are the radius of curvature for the substrate after and before films deposition, respectively, and t_f and t_s are the thickness of the thin films and the substrate, respectively. A laser beam was used to measure the curvature of the Si wafer before and after the film deposition. With the known film thickness as well as the E and ν of the substrate, the films' stress can be obtained.

In the actual measurement, the average radius of curvature for the entire substrate was obtained by scanning 50 points through the laser beam controlled by a program. Young's modulus of substrate was set as 129.5 GPa that is the value for the Si ⟨100⟩ plane. In order to exclude the influence of the edge area of the wafer, the starting and ending points of the scans had a 5 mm offset from the edge of the wafer. Residual stress was obtained by the system after each scan was performed. To obtain the residual stress distribution along different directions of the substrate, the wafer was rotated for 12 different orientations during measurement. The average residual stress for each one sample was calculated by averaging those 12 different values equally.

III. RESULTS

With magnetic sensor applications for the films fabricated in this work, the main properties of interest were the *in situ* magnetic field in relation to films' magnetization behavior and the residual stress that interplays with the films' magnetostrictive

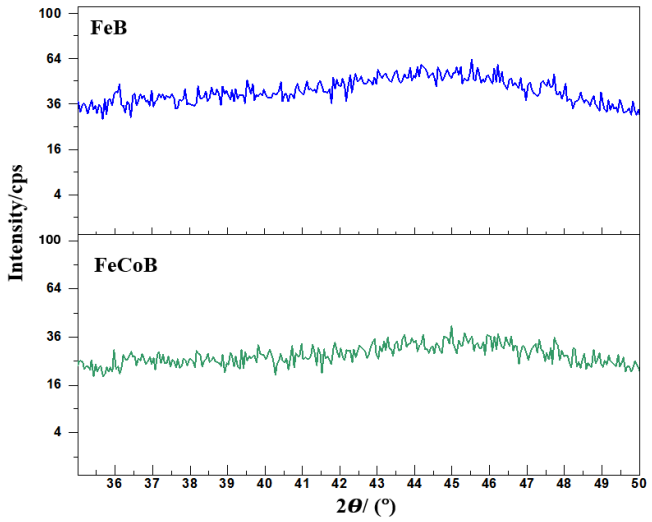

Fig. 3. XRD patterns for FeB and FeCoB films.

properties. In this section, the individual properties measured will be presented with regard to fabrication conditions and the chemical compositions of the films.

As designed, the sputtered films should be amorphous in nature to ensure low coercivity. This was examined first by X-ray diffraction (XRD) as shown in Fig. 3 where we specifically focused on the angle range of 35°–50° for carefully checking the possible crystalline Fe phase. The XRD patterns of both FeB and FeCoB show a broad hump spread across 40°–50° [where the crystalline body centered cubic Fe (110) peak is supposed to be], indicating that those films were amorphous [15], [21], [22]. This was the case for all the films with and without *in situ* field applied. Also, considering the films remained at a low temperature during deposition (<50 °C), it was reasonable to conclude that the deposited films were X-ray amorphous.

Next, magnetic hysteresis loops were measured for all the films. Typical hysteresis loops and the magnetic properties extracted from the loops were summarized and compared in terms of different compositions and deposition conditions. These results are shown in Figs. 4–6. Fig. 4 shows the effect of the *in situ* magnetic field on the FeB films. In Fig. 4(a), applying *in situ* field resulted in an easy axis built into the thin film, which can be seen by the shape difference of the hysteresis loops. The loop of easy axis is not an exact rectangular shape since *in situ* magnetic field cannot completely align the easy axis for as-deposited films [7]. This result means that magnetic moments are not all aligned along easy axis by *in situ* field. It can also be seen from Fig. 4(b) that the coercivity of the FeB film deposited under *in situ* field is smaller than that of the one without *in situ* field applied, whether it is along the easy or the hard axis.

However, due to the very low level of coercivity that is beyond the resolution capabilities of the AGFM, the presence of an *in situ* field did not seem to have the same noticeable effect on FeCoB films as it had on FeB films. This can be seen from Figs. 5 and 6. The coercivity of the FeCoB films was much lower than that of the FeB films, regardless of the application of the *in situ* field. The coercivity for FeB without

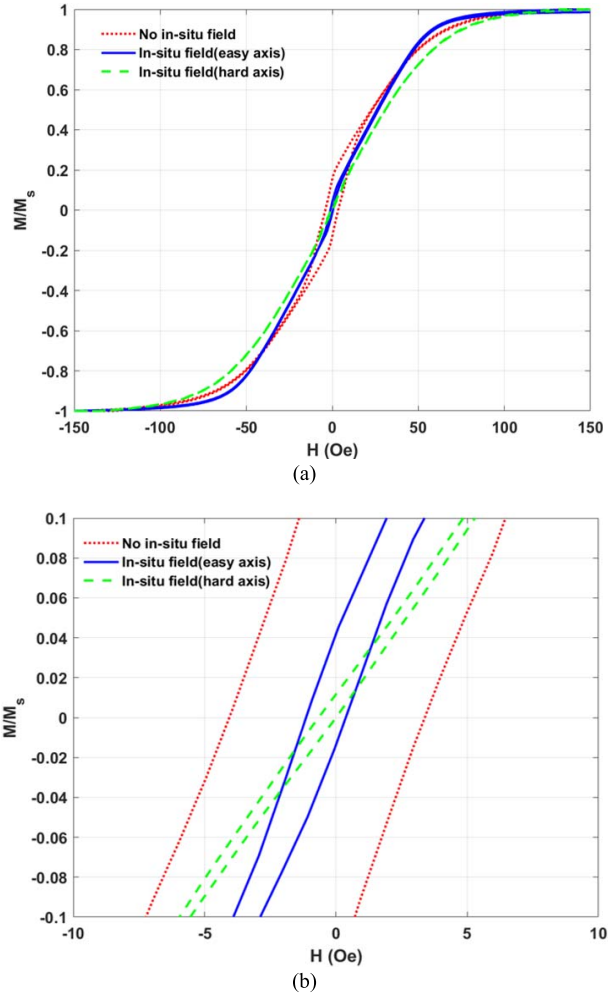

Fig. 4. (a) Hysteresis loops of FeB with/without *in situ* field. (b) Hysteresis loops of FeB with/without *in situ* field at low-field region.

in situ field ranged between 2.5–12 Oe, which was within the range of previously documented studies [14], [23]. The average coercivity was below 0.1 Oe for FeCoB deposited without *in situ* field. Most likely, such difference in the coercivity as summarized in Fig. 6 stem from the compositional difference between FeB and FeCoB, i.e., the addition of Co changed the anisotropy field of thin films. Similar observations were reported in [24]. Also, Fig. 6 reveals that the coercivity of FeB measured along the hard axis is lower than that of measured along easy axis, which is summarized from similar results like Fig. 4.

Since minimizing film residual stress level is an important requirement for the nano/micro fabrication of the intended microelectromechanical system (MEMS) device of this paper, the residual stress of the as-deposited films was measured in detail. The average residual stress for FeB and FeCoB is shown in Figs. 7 and 8. Through tuning the deposition process parameters, the residual stress level can be reduced to below 200 MPa for both FeB and FeCoB. This is in the acceptable range of residual stress control for MEMS applications [25], [26]. At the same depositing conditions, films with thickness 250 nm have the lowest magnitude of residual stress, both for FeB and FeCoB. Also, we found the effect of the *in situ* field on residual stress distribution

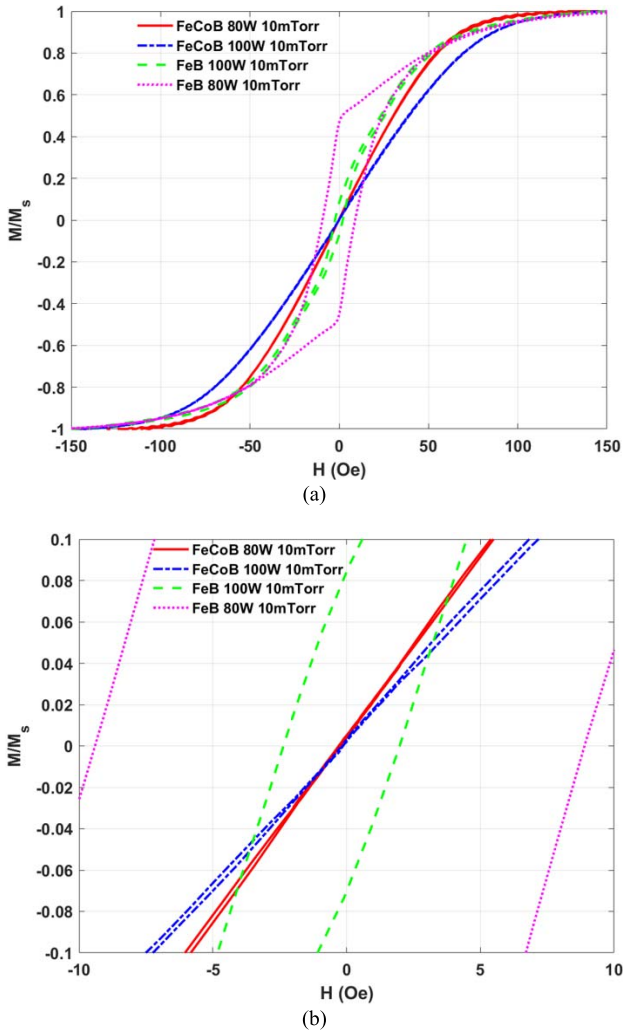

Fig. 5. (a) Hysteresis loops of FeB and FeCoB without *in situ* field. (b) Hysteresis loops of FeB and FeCoB without *in situ* field at low-field region.

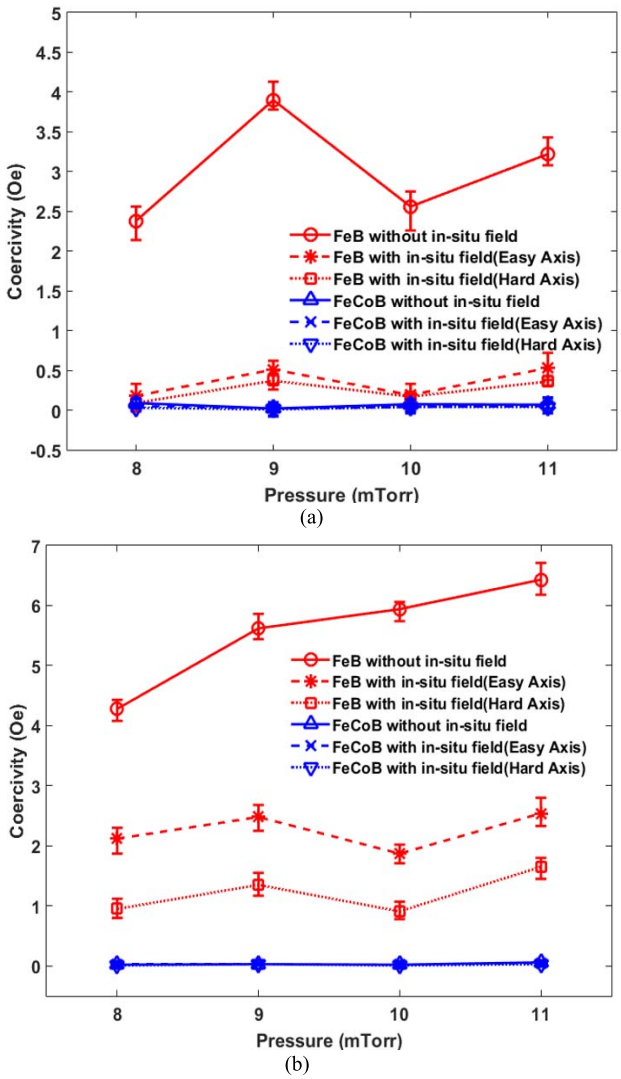

Fig. 6. Coercivity of FeB and FeCoB with/without *in situ* field applied at varying pressure and power of (a) 100 and (b) 120 W.

along different radial directions of the wafer for FeB and FeCoB, by the process of minimizing residual stress, as presented in Figs. 9 and 10. Figs. 9 and 10 were plotted in radar maps with 12 measuring radial directions from 0° to 330° of rotation with respect to the primary flat of the wafer, denoted by the number outside the outermost circle. Fig. 9(a) shows that the *in situ* field has changed the stress distribution to an anisotropic spatial distribution for FeB. Specifically, the stress measured along the direction of *in situ* field applied (easy axis) was larger than that in the direction perpendicular to the *in situ* field direction (hard axis). Also, the hysteresis loops for two samples shown in Fig. 9(a) is presented in Fig. 9(b). The anisotropy for sample with *in situ* field is about 5.95 KJ/m^3. This value is larger than the sample with *in situ* field but showing only isotropic stress distribution, such as the one shown in Fig. 4 by 360 J/m^3. This difference is close to magnetoelastic anisotropy constant of FeB based on its magnetostriction [27] and difference of measured stress between the easy and hard axis. In Fig. 9(c), the four loops represent the stress distribution measured for films deposited with *in situ* field. However, only when the overall stress level dropped to around 20 MPa is the influence on the residual stress distribution observable as an anisotropic feature. As the overall residual stress level increases, this anisotropic feature became difficult to observe. For FeCoB, similar results were also obtained; however, they are more noticeable and unambiguous, as shown in Fig. 10(a). The residual stress difference between the direction along *in situ* field and the direction perpendicular to *in situ* field was about 20 MPa at the thickness of 250 nm, compared to about 8 MPa for FeB for the same thickness. Moreover, this difference increased to about 30 MPa when the film thickness increased to 500 nm, as shown in Fig. 10(b). Considering the average residual stress level of FeCoB, for thicknesses of 250 and 500 nm deposited under the same conditions were about 40–65 MPa (compressive stress) and 50–70 MPa (also compressive), respectively, such directional difference in residual stress cannot be ignored.

IV. Discussion

To ensure the functionality of magnetic sensors, the magnetic and mechanical behavior of the magnetostrictive films need to be optimized. For example in sensing applications, low coercivity of the magnetostrictive films is desired for a

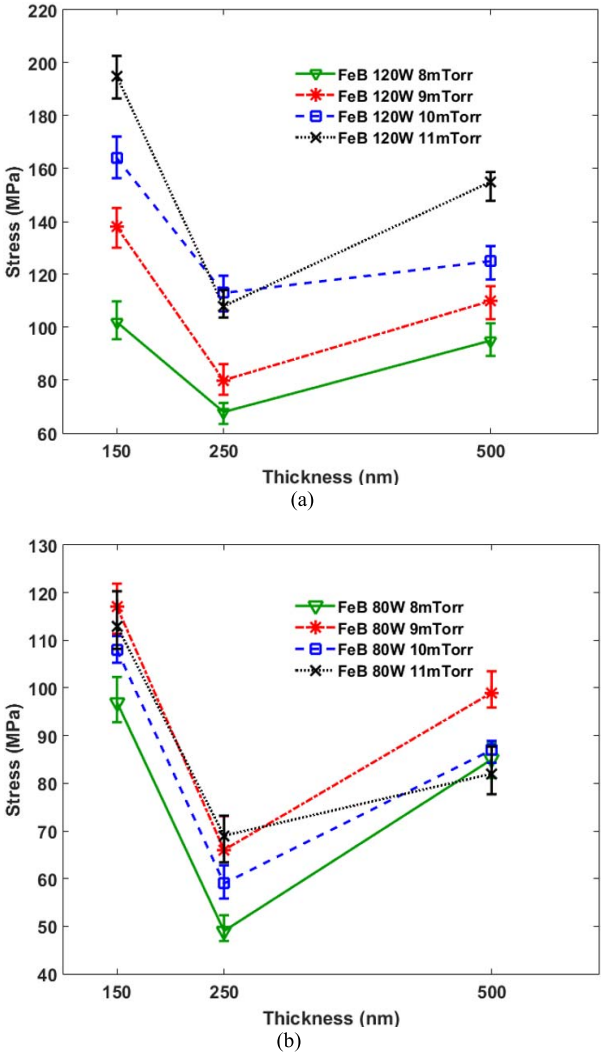

Fig. 7. Average residual stress of FeB without *in situ* field applied at varying thickness and power of (a) 120 and (b) 80 W.

low limit of detection [3]. Also, the residual stress should be optimized for films, for two reasons. On one hand, large residual stress could lead to bending for suspended structures of the magnetic field sensors, and thus adversely affects the magnetoelectric coupling effect [28]. Therefore, a lower residual stress level is preferred for sensors. On the other hand, residual stress could alter the magnetic and magnetostrictive behavior of the thin film due to inverse magnetostrictive effect [27], [29]. Therefore, it is meaningful to study how to optimize the coercivity and residual stress of magnetostrictive thin films from the fabrication perspective. In this paper in particular, the abovementioned properties were also studied with respect to the *in situ* field applied during film deposition for the introduction of magnetic anisotropy for amorphous magnetostrictive films.

First of all, the *in situ* field introduces magnetic anisotropy as shown in the hysteresis loops in Fig. 4(a). When an external magnetic field (H-field) is applied, hysteresis loops measured along the direction of *in situ* field, i.e., along the easy axis, reach saturation at lower H-field than the one measured along the direction perpendicular to *in situ* field, i.e., along the hard axis. This can be explained by the 180° domain wall structure

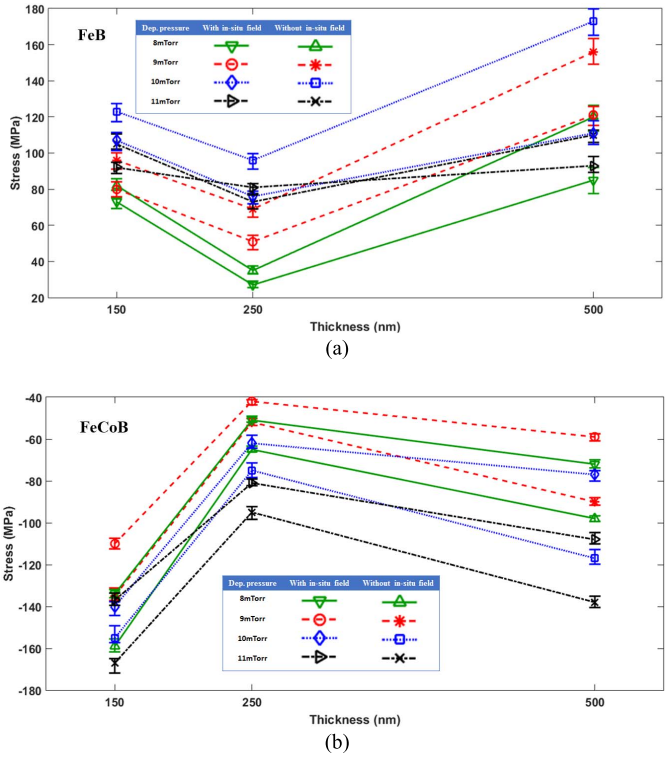

Fig. 8. Residual stress of films deposited with/without *in situ* field at varying thickness and 100 W for (a) FeB and (b) FeCoB.

commonly seen with films deposited with *in situ* film [15]. Such a domain orientation and domain wall structure gives rise to the easy and hard axis within the film.

Second, the *in situ* field also influences the coercivity of the films as shown in Fig. 4(b), which provides two observations: 1) there is an observable coercivty for FeB film deposited with *in situ* field and 2) the FeB films deposited with *in situ* field show a lower coercivity compared with the one without *in situ* field. Let us first discuss the observation 2). One possible explanation for it is the hindrance of the domain wall motion for the following reasons. First of all, domain wall motion dominates magnetization at low H when the magnetostatic energy is relatively small. Also, magnetocrystalline anisotropy obviously cannot be responsible for such non-negligible coercivity and its difference between the easy and hard axis, in an amorphous FeB films [29]. Third, while the domain wall motion can be hindered in many ways, the most likely case in this paper is the microstress due to magnetostriction [29]. More specifically, when an H-field is applied, motion of the domain walls as well that are not parallel to the H-field comes with volume or dimension change due to magnetostriction, which can lead to distortion and buildup of microstress that could hinder the domain wall motion [29]. In the films deposited without an *in situ* field, the orientation of the domains is randomly distributed in all directions, whereas in those deposited with *in situ* field, the domain wall is mostly relatively aligned, forming a domain configuration very close to 180° domains. Therefore, when H-field is applied in the direction parallel to the *in situ* field, the resulting effect is that the domain walls can move more freely, which manifests as a lower coercivity.

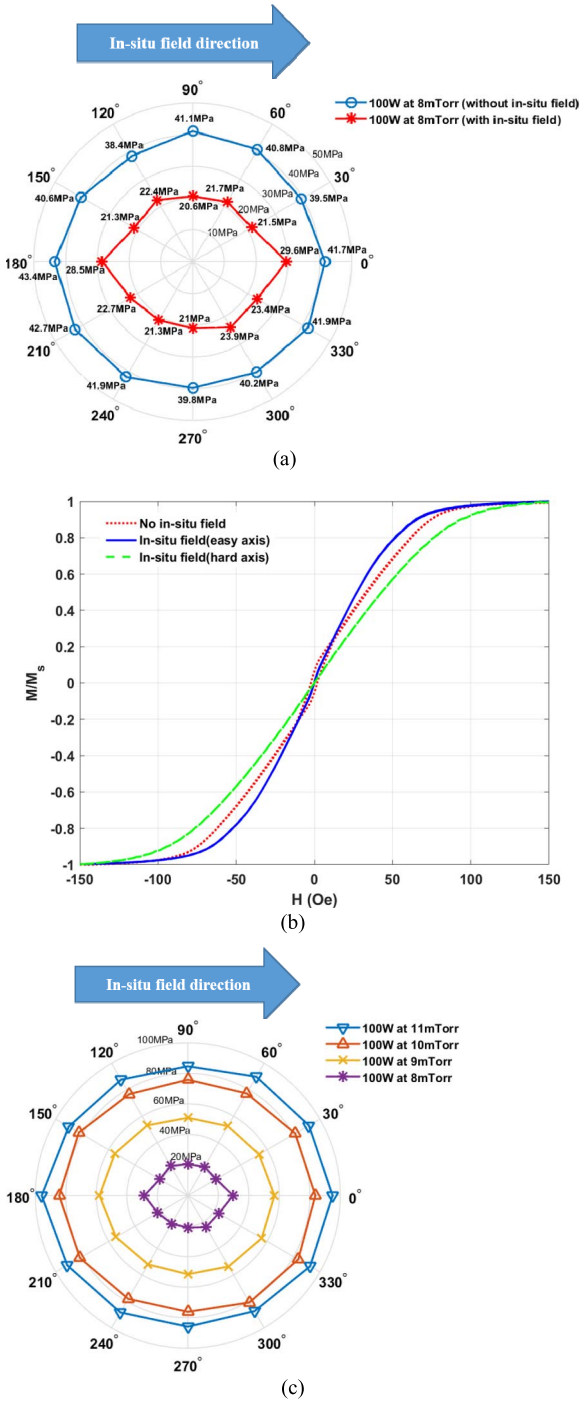

Fig. 9. Residual stress distribution across different directions for FeB at 250 nm thickness. (a) Effect of *in situ* field on stress distribution. (b) Hysteresis loops of FeB samples in (a). (c) Effect of different overall residual stress level on stress distributions.

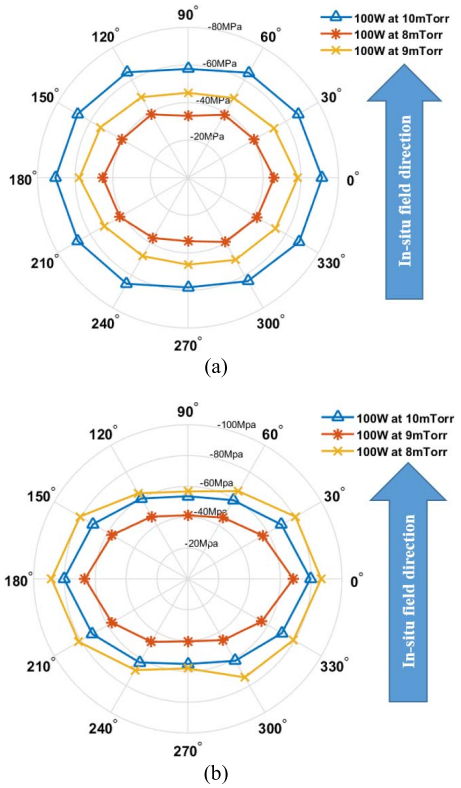

Fig. 10. Residual stress distribution across different directions for FeCoB at thickness of (a) 250 and (b) 500 nm.

As for the observation 1), the observable coercivity for FeB films with *in situ* field especially for the one measured along easy axis in fact showed the likely presence of the domains that were not completely aligned by the *in situ* field during deposition, which has been observed in other studies as well [5]. As a result, motion of such domain walls in FeB films with *in situ* field can encounter some hindrance and result in a net coercivity. The fact that the FeB films deposited with *in situ* field show a lower coercivity compared with the one without *in situ* field, as shown in Figs. 4 and 6, shows that *in situ* field did effectively produced domain wall structure close to ideal 180° domain wall even though not all of magnetic moments are aligned along the easy axis.

In addition to controlling the coercivity, optimization of the residual stress for magnetostrictive films is also essential because of the inverse magnetostrictive effect. In this paper, the potential thermal stress [20] was minimized by using a relative low RF power for sputtering, as well as implementing carefully designed alternating sputter and cooling cycles during deposition that ensured the substrate temperature was kept below 50 °C.

During the process of locating the depositing conditions of lowest residual stress at different thicknesses, it is observed that the *in situ* field affected the distribution of the residual stress over different directions when the overall residual stress is below a certain level, as shown in Figs. 9 and 10. While the stress distribution for the film deposited without *in situ* field was relatively isotropic, that of the films deposited with *in situ* field showed a noticeable anisotropy that evidently was related to the application of *in situ* field. Even though this anisotropy existed, it was fairly small.

As a result of the extra stress due to *in situ* field, the magnetic anisotropy of magnetostrictive films should include the magnetoelastic energy. Therefore, the magnetization behavior of films must change accordingly. For example, considering a single-domain particle with its easy axis along the y-axis and subjected to a bi-axial stress, we can magnetize it through a hard-axis magnetizing process which is shown in Fig. 11.

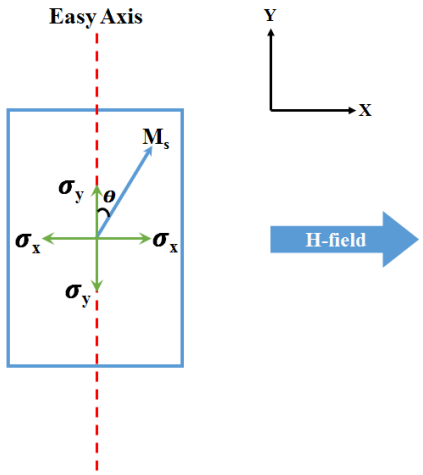

Fig. 11. Schematic of the rotation of magnetization for a single domain with subject to H-field and bi-axial stress.

In Fig. 11, M_s is the vector magnetization and θ is the tilted angle of M_s away from its easy axis as the H-field is applied, and σ_x and σ_y are the stresses along the X and Y directions respectively. The change of the free energy density of the system U_{sys} can be written by summing the uniaxial anisotropy energy density due to the *in situ* field, U_a, magnetostatic energy due to the applied H-field, U_m, and magnetoelastic energy density U_{me} as represented in the following equations:

$$U_{\text{sys}} = U_a + U_m + U_{me} \tag{1}$$

$$U_a = K_a \sin^2\theta \tag{2}$$

$$U_m = -\mu_0 M_s H \sin\theta \tag{3}$$

$$U_{me} = (3/2)\lambda_s \sigma_x \cos^2\theta + (3/2)\lambda_s \sigma_y \sin^2\theta \tag{4}$$

where K_a is the uniaxial magnetic anisotropy constant just due to *in situ* field and μ_0 is magnetic permeability of vacuum. λ_s is saturation magnetostriction coefficient of material. When the system reaches saturation state, we can write the anisotropy field H_a as in (5), by setting the derivative of U_{sys} with respect to θ to be 0 and take θ to be 90° [27]

$$H_a = \frac{2K_a + 3\lambda_s(\sigma_y - \sigma_x)}{\mu_0 M_s}. \tag{5}$$

Equation (5), which is different from the usual equation for anisotropy field ($H_a = 2K_a/(\mu_0 M_s)$ [29]), implies that difference of stress between X and Y directions can affect the value of H_a. If this stress difference and λ_s is positive, such as bi-axial stress in tensile state and $\sigma_x < \sigma_y$, or in compressive state and $|\sigma_x| > |\sigma_y|$, the already existing magnetic anisotropy can be reinforced by magnetoelastic energy and hence results in a higher anisotropy field. On the contrary, if this stress difference is negative, the original magnetic anisotropy could be weakened and make material easier to magnetize. It should be noted that (5) can be used for any films that are subjected to bi-axial stress if σ_x and σ_y can be measured. More importantly, the magnitude level of the term $3\lambda_s(\sigma_y - \sigma_x)$ could be roughly estimated at several hundred J/m^3 based on common value of saturation magnetostriction coefficient for Fe-based materials [27] and the extra stress level measured in this paper. This level is comparable to $2K_a$ [14], [23], and hence cannot be ignored when we optimize magnetostrictive films for magnetic field sensor or actuator or design related device, even though the exact value of such magnetoelastic energy would be hard to measure in actual situation for thin films. Therefore, such anisotropic distribution of residual stress can interplay with magnetic anisotropy already built within films, and hence affect magnetic properties and behaviors of films a great deal.

V. Conclusion

In this paper, properties of FeB and FeCoB thin films such as coercivity and residual stress were investigated with respected to the *in situ* field applied during deposition by experimental and theoretical analysis. Such properties manifest themselves in the magnetic and the mechanical behaviors of the magnetostrictive films, which are crucial for the application of the films in magnetic field sensors or actuators. Their influences can be summarized into the following two aspects.

1) An *in situ* magnetic field applied during deposition can be beneficial to the reduction of the coercivity of the magnetostrictive films.
2) An *in situ* magnetic field can result in an extra uniaxial residual stress in the FeB and FeCoB films, which could add a magnetoelastic anisotropy that is enough to affect the overall magnetic anisotropy of films.

Acknowledgment

This work was supported in part by the CMU-SYSU Collaborative Innovation Research Center and in part by the SYSU-CMU Shunde International Joint Research Institute. The work of S. Wang and J. Zhu was supported in part by "Pearl River Talent Plan" 5th Innovation Team of Guangdong Province under Grant 2014ZT05D340 and in part by the Special Project of Applicable Science and Technology of Guangdong Province under Grant 2015B010129010.

References

[1] E. Quandt, S. Stein, and M. Wuttig, "Magnetic vector field sensor using magnetoelectric thin-film composites," *IEEE Trans. Magn.*, vol. 41, no. 10, pp. 3667–3669, Oct. 2005.
[2] D. Burdin, D. Chashin, N. Ekonomov, L. Fetisov, Y. Fetisov, and M. Shamonin, "DC magnetic field sensing based on the nonlinear magnetoelectric effect in magnetic heterostructures," *J. Phys. D, Appl. Phys.*, vol. 49, no. 37, p. 375002, 2016.
[3] F. T. Calkins, A. B. Flatau, and M. J. Dapino, "Overview of magnetostrictive sensor technology," *J. Intell. Mater. Syst. Struct.*, vol. 18, no. 10, pp. 1057–1066, 2007.
[4] T. Nan, Y. Hui, M. Rinaldi, and N. X. Sun, "Self-biased 215 MHz magnetoelectric NEMS resonator for ultra-sensitive DC magnetic field detection," *Sci. Rep.*, vol. 3, Jun. 2013, Art. no. 1985.
[5] Y. Hui, T. Nan, N. X. Sun, and M. Rinaldi, "High resolution magnetometer based on a high frequency magnetoelectric MEMS-CMOS oscillator," *J. Microelectromech. Syst.*, vol. 24, no. 1, pp. 134–143, Feb. 2015.
[6] S. Marauska, R. Jahns, H. Greve, E. Quandt, R. Knöchel, and B. Wagner, "MEMS magnetic field sensor based on magnetoelectric composites," *J. Micromech. Microeng.*, vol. 22, no. 6, p. 065024, 2012.
[7] H. Greve, E. Woltermann, H.-J. Quenzer, B. Wagner, and E. Quandt, "Giant magnetoelectric coefficients in $(Fe_{90}Co_{10})_{78}Si_{12}B_{10}$-AlN thin film composites," *Appl. Phys. Lett.*, vol. 96, no. 18, p. 182501, 2010.
[8] M. A. Mitchell, A. E. Clark, H. T. Savage, and R. J. Abbundi, "ΔE effect and magnetomechanical coupling factor in $Fe_{80}B_{20}$ and $Fe_{78}Si_{10}B_{12}$ glassy ribbons," *IEEE Trans. Magn.*, vol. MAG-14, no. 6, pp. 1169–1171, Nov. 1978.

[9] L. Yin-Chih, "Microstructures and magnetostrictive strains of Fe-Ga-Ni ferromagnetic shape memory alloys," *J. Appl. Phys.*, vol. 113, no. 17, p. 17A303, 2013.

[10] J. B. Restorff, M. Wun-Fogle, K. B. Hathaway, A. E. Clark, T. A. Lograsso, and G. Petculescu, "Tetragonal magnetostriction and magnetoelastic coupling in Fe-Al, Fe-Ga, Fe-Ge, Fe-Si, Fe-Ga-Al, and Fe-Ga-Ge alloys," *J. Appl. Phys.*, vol. 111, no. 2, pp. 023905-1–023905-12, 2012.

[11] M. D. Moffett *et al.*, "Characterization of Terfenol-D for magnetostrictive transducers," *J. Acoust. Soc. Amer.*, vol. 89, no. 3, pp. 1448–1455, 1991.

[12] A. Ludwig and E. Quandt, "Optimization of the ΔE effect in thin films and multilayers by magnetic field annealing," *IEEE Trans. Magn.*, vol. 38, no. 5, pp. 2829–2831, Sep. 2002.

[13] X. Liu and X. Zheng, "A nonlinear constitutive model for magnetostrictive materials," *Acta Mech. Sinica*, vol. 21, no. 3, pp. 278–285, 2005.

[14] I. Fernández-Martínez, J. L. Costa-Krämer, and F. Briones, "Stress and magnetoelastic properties control of amorphous $Fe_{80}B_{20}$ thin films during sputtering deposition," *J. Appl. Phys.*, vol. 103, no. 11, p. 113902, 2008.

[15] Y. Lu and A. Nathan, "Metglas thin film with as-deposited domain alignment for smart sensor and actuator applications," *Appl. Phys. Lett.*, vol. 70, no. 4, p. 528, 1997.

[16] T. Morikawa, Y. Nishibe, H. Yamadera, Y. Nonomura, M. Takeuchi, and Y. Taga, "Giant magneto-impedance effect in layered thin films," *IEEE Trans. Magn.*, vol. 33, no. 5, pp. 4367–4372, Sep. 1997.

[17] A. Bechert, R. Trautsch, J. Zweck, W. Andrä, and H. Hoffmann, "Influence of field-annealing on the magnetic anisotropy of amorphous Fe–Tb films," *Phys. Status Solidi A*, vol. 161, no. 2, pp. 483–492, 1997.

[18] J. Lou, R. E. Insignares, Z. Cai, K. S. Ziemer, M. Liu, and N. X. Sun, "Soft magnetism, magnetostriction, and microwave properties of FeGaB thin films," *Appl. Phys. Left.*, vol. 91, p. 182504, Oct. 2007.

[19] J. Gao *et al.*, "The effect of boron addition on the atomic structure and microwave magnetic properties of FeGaB thin films," *J. Appl. Phys.*, vol. 105, no. 7, p. 07A323, 2009.

[20] L. B. Freund and S. Suresh, *Thin Film Materials Stress, Defect Formation and Surface Evolution*. Cambridge, U.K.: Cambridge Univ. Press, 2004, p. 67.

[21] J. W. Hong, H. S. Shin, T. S. Jang, and J. W. Park, "Magnetic properties of $Fe_{1-x}B_x$ (0 = x = 0.2) films prepared by dc magnetron sputtering," *J. Korean Phys. Soc.*, vol. 42, no. 5, pp. 612–615, 2003.

[22] J. Díaz, C. Quirós, and L. M. Alvarez-Prado, "Determination of the magnetostrictive atomic environments in FeCoB alloys," *Phys. Rev. B, Condens. Matter*, vol. 85, no. 13, p. 134437, 2012.

[23] I. Fernández-Martinez *et al.*, "Nitrided FeB amorphous thin films for magneto mechanical systems," *J. Magn. Magn. Mater.*, vol. 320, no. 1, pp. 68–75, 2008.

[24] A. T. Hindmarch, A. W. Rushforth, R. P. Campion, C. H. Marrows, and B. L. Gallagher, "Origin of in-plane uniaxial magnetic anisotropy in CoFeB amorphous ferromagnetic thin films," *Phys. Rev. B, Condens. Matter*, vol. 83, p. 212404, Jun. 2011.

[25] G. Piazza, "Piezoelectric aluminum nitride vibrating RF MEMS for radio front-end technology," Ph.D. dissertation, Dept. Eng. Elect. Eng. Comput. Sci., Univ. California, Berkeley, Berkeley, CA, USA, 2005, p. 97.

[26] E. Herth, E. Algré, J. Y. Rauch, J. C. Gerbedoen, N. Defrance, and P. Delobelle, "Modeling and characterization of piezoelectric beams based on an aluminum nitride thin-film layer," *Phys. Status Solidi A*, vol. 213, no. 1, pp. 114–121, 2016.

[27] R. C. O'Handley, *Modern Magnetic Materials: Principles and Applications*. New York, NY, USA: Wiley, 2000, pp. 221–227.

[28] M. Fiebig, "Revival of the magnetoelectric effect," *J. Phys. D, Appl. Phys.*, vol. 38, no. 8, p. R123, 2005.

[29] B. D. Cullity and C. D. Graham, *Introduction to Magnetic Materials*, 2nd ed. Piscataway, NJ, USA: IEEE Press, 2009, pp. 258–265, 305–308, and 312–316.